A novel control strategy for enhancing biological N-removal in a granular sequencing batch reactor: a model-based study

Eduardo Isanta[a], Mónica Figueroa[b], Anuska Mosquera-Corral[b], Luis Campos[b], Julián Carrera[a], Julio Pérez[a]*

[a]Department of Chemical Engineering, Escola d'Enginyeria, Universitat Autònoma de Barcelona, Spain

[b]Department of Chemical Engineering, School of Engineering, University of Santiago de Compostela, Spain

*Corresponding author. Phone: +34935812141; Fax: +34935812013

e-mail: julio.perez@uab.cat

Abstract

Biological nitrogen removal in aerobic granular sequencing batch reactors is sensitively affected by process conditions (e.g. dissolved oxygen (DO) concentration, nitrogen loading rate (NLR), influent C/N ratio, among others). The variation of one of these process conditions affects the others, because often they are tightly linked. These interrelationships are a drawback for the experimental assessment of the target domain of process conditions required to enhance N-removal. Here, we have developed a model to determine the guidelines to design an automatic control strategy with the final aim of enhancing biological N-removal in a granular sequencing batch reactor. The model was first calibrated with experimental data from a granular sequencing batch reactor treating

Abbreviations: AOB, Ammonium-oxidizing Bacteria; ASM3, Activated Sludge Model No.3; COD, Chemical Oxygen Demand; DO, Dissolved Oxygen; GSBR, Granular Sequencing Batch Reactor; N, Nitrogen; NOB, Nitrite-oxidizing Bacteria.

swine wastewater. Specific simulations were designed to elucidate the effect of DO concentration (0.5 – 8 mg O_2 L^{-1}), granule size (0.5 – 3.5 mm), influent C/N ratio (4 – 10 g O_2 g^{-1} N) and NLR (0.41 – 0.82 g N L^{-1} d^{-1}) on the nitrification-denitrification efficiency. Simulation results showed that, in general, high N-removal efficiencies (from 70 to 85 %) could be obtained only setting the appropriate DO concentration. That appropriate DO concentration could be easily found based on effluent ammonium concentration. Those results were used to propose a control strategy to enhance N-removal efficiencies. The control strategy was based on a closed DO loop with variable DO set-point. The DO set-point was established at a constant value for the whole cycle (i.e. once per cycle), based on the on-line measurement of ammonium concentration at the end of the previous cycle.

Keywords

Aerobic granular sludge; Dissolved oxygen concentration; Mathematical modeling; Nitrification-denitrification; On-line ammonium concentration; Particle size.

Nomenclature

μ_D	Diffusivity reduction factor
$\mu_{max,i}$	Maximum growth rate of i population (d^{-1})
C/N	Chemical Oxygen Demand to Nitrogen ratio (g O_2 g^{-1} N)

DO_{opt}	DO concentration maximizing N-removal for a given conditions (mg O_2 L^{-1})
HRT	Hydraulic Retention Time (d)
k_{STO}	Maximum storage rate constant of heterotrophic bacteria (d^{-1})
NLR_s	Specific Nitrogen Loading Rate (g N L^{-1} d^{-1})
NLR_v	Volumetric Nitrogen Loading Rate (g N L^{-1} d^{-1})
r	Simulated granule radius (m)
R_m	Experimental mean radius (m)
S_i	Concentration of the soluble compound i (mg L^{-1})
SRT	Sludge Retention Time (d)
u_{Det}	Biofilm detachment rate (m d^{-1})
u_F	Biofilm growth velocity (m d^{-1})
VSS	Volatile Suspended Solids concentration (mg L^{-1})
X_i	Concentration of the particulate compound i (mg L^{-1})

1. Introduction

Recently, aerobic granular sequencing batch reactors (GSBR) have been successfully used for the treatment of municipal and industrial wastewater effluents [1 – 7]. Granules have a compact, dense and thick structure which provides good settling and retention capacities [8 – 9]. Granular sludge reactors operate at higher loading rates using more

compact reactor designs, if compared with activated sludge [10 – 12]. Moreover, the morphological structure of aerobic granular sludge provides the existence of substrate profiles across the granule depth, enabling simultaneous aerobic and anoxic processes into the same bioparticle. For these reasons, GSBRs have shown a very good performance in organic matter and nitrogen (N) removal [10, 13 – 14].

High N-removal is achieved when the aerobic and anoxic zones of the granules are correctly balanced [15]. This balance depends on many variables, some of them are associated to the granules characteristics (i.e., particle size, density, porosity), whereas others are related to the operational conditions of the reactor (DO concentration, NLR, influent C/N ratio). Experimental campaigns devoted to study the individual effect of these variables is often very challenging and time-consuming, since a change in one of them may affect the others. For example, studying the effect of influent loading rate over nutrients removal efficiency may be affected by variations in the size of the granules [16]. Also, changing the DO concentrations manipulating the air-flow rate may also cause a change in the density of the granules [17]. Therefore, it is difficult to experimentally assess, in an independent manner, the effects of each variable on N-removal efficiency. Furthermore, some parameters, especially those related to biomass characteristics, are not easy to control and tend to fluctuate even in steady state [12,18], hindering its study.

Automatic control strategies are a good tool both for optimization of the performance of wastewater treatments and to apply corrective actions in front of influent or biomass disturbances [19]. Two operational modes are commonly reported for N-removal with aerobic granular sludge: i) GSBRs with a completely aerated reaction phase [6,10,12,14]. In that operational mode, simultaneous nitrification-denitrification is the main N-removal pathway and ii) GSBRs with one or several anoxic periods

[5,18,20,21]. These anoxic periods are introduced for enhancing denitrification. Although, in general, these configurations showed good N-removal performance, none of these studies used automatic control strategies. In fact, the use of automatic control strategies in GSBRs is still scarce. Some of the examples are: (i) to control the length of cycle as a function of the ammonium concentration for nitritation of high-strength ammonium wastewaters with a very low influent C/N ratio [22]; (ii) to control the length of the cycle by means of ORP, DO and pH curves for winery [23] and synthetic wastewaters [24].

To overcome the challenges associated to experimental set-ups, the mathematical modeling has been proven to be a useful tool for analyzing complex systems, such as the GSBR. In that sense, some researchers developed mathematical models describing the COD and N-removal via the nitrification and heterotrophic denitrification processes [13, 25,26]. De Kreuk et al. [15] introduced the biological phosphorus removal and studied the individual influence of some parameters (i.e. temperature and granule size) over the nutrient removal. Vazquez-Padín et al. [27] showed that the biomass characteristics could be successfully described if a porosity profile across the granules depth was taken into account. Later, Su et al. [28] modeled the variations in size and density of granules due to growth, detachment or breakage, to optimize the size and density of granules.

Most of the efforts of these studies were focused on understanding the behavior of the GSBR, but not in finding the best practical strategy to be implemented with the aim to improve the N-removal. In this study, a mathematical model describing the steady state operation of a GSBR treating diluted swine wastewater was calibrated and validated with different sets of experimental data. This model was then exploited to assess the impact of easily measurable parameters on the N-removal efficiency. The selected

parameters were DO concentration, granule size, NLR and influent C/N ratio. From the results of the exploitation, a control strategy to improve the N-removal in GSBRs was proposed and evaluated through modeling.

2. Materials and Methods

2.1 Characteristics of the GSBR operation

Experimental data for the modeling were obtained from a 1.5 L GSBR treating diluted swine wastewater. The reactor cycles were distributed as fill (3 min), aeration (171 min), settling (1 min) and discharge (5 min). The hydraulic retention time was 6 h. The reactor was operated at room temperature (23 ± 2 ºC), while the pH was not controlled and ranged from 7.5 – 8.5. Air was supplied through an air diffuser at the bottom of the reactor at a constant flow-rate (3.5 L min^{-1}), and the DO concentration varied in the range 2 – 6 mg O_2 L^{-1}.

Activated sludge collected from a municipal WWTP was used as inoculum. Five days after the start-up most of the inoculum biomass washed out from the reactor and first granules appeared. On day ten, the average diameter of the granular biomass was 1.87 mm and the volatile solids content inside the reactor was 1.27 g VSS L^{-1} [6].

After the start-up, the GSBR operational strategy consisted in stepwise decrease of the dilution ratio of the swine wastewater with tap water. Experimental data from the operational periods A and C from the GSBR (see Fig. 1) were used for modeling purposes. In period A, the dilution ratio of swine wastewater with tap water was 1:25, resulting in an influent composition of 600 mg O_2 L^{-1} of readily-biodegradable chemical oxygen demand (COD), 60 mg O_2 L^{-1} of non-biodegradable COD and 103 mg N L^{-1} of

ammonium (table 1). For period C, the dilution ratio of swine wastewater with tap water was 1:15, resulting in an influent composition of 1000 mg O_2 L^{-1} of readily-biodegradable COD, 116 mg O_2 L^{-1} of non-biodegradable COD and 200 mg N L^{-1} of ammonium (table 1). More details about the performance of the reactor can be found in Figueroa et al. [6].

3. Model development

The modeling platform used to develop the mathematical model was AQUASIM [29]. The biofilm reactor compartment (based on Reichert [29] mixed-culture biofilm model) provided by AQUASIM was used to simulate the mass transfer and biological conversion processes occurring in the granules. The description of the biofilm in AQUASIM is one-dimensional, and only the perpendicular direction to the substratum is resolved [29].

3.1 Biological processes

The model included six soluble compounds: oxygen (S_{O2}), ammonium (S_{NH4}), nitrite (S_{NO2}), nitrate (S_{NO3}), readily-biodegradable organic substrate (S_S) and non-biodegradable organic substrate (S_I); and five types of particulate compounds: ammonium-oxidizing bacteria (X_A), nitrite-oxidizing bacteria (X_N), heterotrophic bacteria (X_H), storage products (X_{STO}) and inert particulate organic material (X_I). Kinetics and stoichiometry of the biological processes were defined using the Activated Sludge Model No.3 (ASM3) platform [30]. However, the ASM3 presents several limitations for describing systems operating in batch mode or with nitrite accumulation. To overcome these limitations, two modifications were introduced: (i) the model considered simultaneous growth and storage of organic matter by heterotrophic bacteria as described by Sin et al. [31], (ii) nitrite was included as nitrification intermediate as

described by Jubany et al. [32], since there was an evident accumulation of nitrite in the GSBR (Fig. 1). Therefore, nitrification becomes a two-step process. Firstly, ammonium is oxidized to nitrite by ammonium-oxidizing bacteria (AOB), and secondly, nitrite is oxidized to nitrate by the nitrite-oxidizing bacteria (NOB). Furthermore, since nitrite was included in the model, all the anoxic processes, heterotrophic and autotrophic, (i.e. AOB and NOB endogenous respiration) were possible either from nitrite or from nitrate [33]. Separate anoxic reduction factors were used for X_A, X_N and X_H [33]. Additionally, the anoxic processes from nitrate had a lower reduction factor to avoid an overall denitrification rate higher than the aerobic consumption rate of COD [33].

The hydrolysis of slowly biodegradable COD (X_S) to S_S by X_H was not taken into account. Given that the raw swine wastewater was stored several weeks without continuous mixing before being diluted and entering the reactor, it was considered that most of X_S decanted in the storage tank. Therefore, the overall impact of the hydrolysis of the remaining X_S on the behavior of the GSBR was considered negligible. Further details of kinetics and stoichiometry of the developed model are summarized in Tables S1, S2 and S3 in Supporting Information.

3.2 SBR operation

To simulate the feeding and effluent withdrawal periods of the GSBR, the biofilm reactor compartment was linked to a completely mixed liquid compartment whose volume can vary during the simulation (Fig. S1 in Supporting Information; see Vazquez-Padín et al. [27] for further details). The completely mixed compartment received the feeding and effluent withdrawal operations. The biofilm reactor had a constant volume (0.75 L) and contained the total amount of granules and part of the bulk liquid. The rest of the bulk liquid was in the completely mixed reactor

compartment (0.76 L). Both compartments were interconnected with a recirculation flow-rate to ensure good liquid mixing.

In the experimental set-up, during the periods without mixing (settling, discharge and feeding), the mass transfer of soluble compounds from the bulk liquid to the biofilm pore water becomes reduced, resulting in a lower biological activity of the granules. Furthermore, the GSBR was fed from the top of the reactor; therefore, the settled granules did not mix with the new media until the aeration started. To mimic the real operation of the reactor, a reduction factor applied to the diffusivity of soluble compounds into the pore water of granules (similarly to De Kreuk et al. [15]) was used with the aim to minimize the biological reactions during the non-aerated periods. This reduction factor was noted as μ_D.

3.3 Granules description

Biofilm area was described as a function of the granule radius, to correctly simulate the biofilm geometry. Total biofilm area was defined as a function of granule size and number of granules (see Jemaat et al. [34] for further details). The granule size used as model input was the volume-weighted average diameter experimentally determined in the lab-reactor. The number of granules was determined dividing the total volume of granules by the volume of a single granule, taking into account the experimentally determined density and total solids concentration. As in Vazquez-Padín et al. [27], a detachment rate (u_{Det}) was used to keep a constant biofilm thickness in steady state at a predefined value (Eq. 1).

$$u_{Det} = \left(\frac{r - R_m}{R_m} \cdot 100 + 85 \right) \cdot u_F, \quad \textit{if } u_F > 0, \textit{ otherwise} \quad u_{Det} = 0 \tag{1}$$

Being u_F the growth velocity of the granules (m d^{-1}), r the simulated granule radius (m) and R_m the experimental mean radius (m). Attachment of biomass onto the biofilm surface has been neglected. For the sake of simplicity external mass transfer has been neglected. The porosity of the biofilm was fixed as 80% and kept constant during all the simulations.

3.4 Model calibration and validation strategy

The operational conditions applied for period A as well as the biomass characteristics at the end of that period were used to calibrate the model (Table 1). Then, the concentrations of N-compounds and COD of a simulated cycle in steady-state were compared with an experimental cycle of the GSBR at the end of this period. To ensure steady conditions, each simulation lasted for at least 148 days, corresponding to 20 h of computing time on an Intel Core2Quad CPU at 2.66GHz. Results in terms of biofilm (biofilm thickness and biomass fractions in the biofilm depth) and N-compounds concentrations in the bulk liquid were inspected to check that constant values were achieved.

The same procedure was applied for validation, but using the experimental conditions and biomass characteristics of period C (Table 1) and the same kinetic and stoichiometric parameters than in calibration (Table S2 in Supporting Information). The wastewater treated in period C had a slightly lower influent C/N ratio to that in the calibration (period A) but the NLR and organic loading rate were almost double. Due to these differences, the selection of this operational period for validation purposes is justified.

3.5 N-removal assessment strategy

For the assessment of the N-removal in the GSBR, four relevant and easily measurable parameters at industrial scale (DO concentration, granule size, NLR and influent C/N ratio) were selected, seeking to improve operational strategies. With that purpose, five scenarios were defined: Period A, C/N_Low, C/N_High, NLR_1.5 and NLR_2.0 (Table 2). Period A scenario presented the characteristics of the GSBR operation in the experimental period A (Fig. 1). For scenarios C/N_Low, C/N_High, the conditions of Period A were taken as a basis, and the influent COD was modified to obtain an influent C/N ratio of 4 g O_2 g^{-1} N (C/N_Low) and 10 g O_2 g^{-1} N (C/N_High). For scenarios NLR_1.5 and NLR_2.0, the conditions of period A were also taken as modeling basis, and the length of the cycle time was modified to 120 min (NLR_1.5) and 90 min (NLR_2.0) to increase the applied NLR. The reduction of the cycle time was applied to the aerobic phase, keeping the same feeding, settling and discharge times used in period A.

The conditions of each scenario were simulated until steady state for different DO concentrations and granule sizes. Four different granule sizes were used (0.5, 1.0, 2.0 and 3.5 mm) to cover the typical range of granule sizes found in the literature [6, 10, 12, 18]. Regarding the DO variations, six different DO concentrations, between 0.5 and 8 mg O_2 L^{-1}, were tested. DO concentrations lower than 0.5 mg L^{-1} were not used since they are not expected to be applied in a real GSBR [14,35]. The combination of both variables resulted in 24 different simulations for every scenario. For easy comparison between scenarios, the simulations were performed with the same volume (and mass) of granules. Therefore, the number of granules used in each simulation was set according to the selected granule size.

4. Results and Discussion

4.1 Model calibration

All kinetic parameters were obtained from the bibliography with the exception of the maximum growth rate of X_H ($\mu_{max,H}$), the maximum growth rate of X_A ($\mu_{max,A}$) and the storage rate constant (k_{STO}), that were determined to provide a good description of N-compounds and COD concentration. For the sake of simplicity, the maximum growth rate of X_N ($\mu_{max,N}$) was assumed to be equal to $\mu_{max,A}$, as expected at the temperature used in the experiments (23 ± 2 ºC) [36]. Best results were obtained for a $\mu_{max,H}$ of 5.2 d^{-1}, a $\mu_{max,A}$ of 1.32 d^{-1} and a k_{STO} of 13.2 d^{-1}. All three values were slightly higher than the typical values found in the literature for conventional wastewater treatment plants (2 – 3 d^{-1}, 0.8 – 1.1 d^{-1} and 5 – 12 d^{-1}, respectively [30, 33]). However, maximum growth rates are known to be higher in reactors with alternating feast-famine conditions, as the GSBR here modeled. In fact, Munz et al. [37] found that $\mu_{max,A}$ ranged from 0.9 - 1.4 d^{-1} at 20 ºC for an SBR with the abovementioned conditions.

Apart from these three kinetic parameters, the diffusivity reduction factor (μ_D, section 3.2) was also calibrated. Several values of μ_D were tested in previous simulations and best results were obtained for a μ_D of 0.01 (Fig. 2).

The profiles of COD, ammonium, nitrite and nitrate predicted by the calibrated model are shown in Figs. 3A and 3B. During the first 20 min of the cycle, COD was consumed (feast phase) and the nitrate remaining from the previous cycle was denitrified. The use of the μ_D factor was crucial for a correct description of the COD concentration just after the feeding phase (Fig. 2). During the famine phase (after the COD consumption), the nitrification became the main biological process. Nitrate was the nitrification product, although a slight accumulation of nitrite occurred from minute 30 to 150 (Fig. 3A). The model was able to correctly describe all the processes occurring during the cycle. First, the COD consumption and subsequent denitrification of the nitrate occurring during the

feast phase. And second, the nitrification and nitrate accumulation during the famine phase. Also the nitrite accumulation was adequately predicted by the model, although this accumulation was slightly higher than the experimentally observed. However, the N-total was correctly described by the model.

4.2 Model validation

In the experimental cycle from period C used for the model validation, COD was consumed during the first minutes of the cycle and all the nitrate and nitrite remaining from the previous cycle were denitrified. However, this feast phase was longer than in period A, since lasted for 30 min (Fig. 3D). During the famine phase, ammonium was not fully consumed, since a final accumulation of 10 mg $N\text{-}NH_4^+ L^{-1}$ was observed. Nitrate and nitrite at the end of the cycle were similar. The model correctly described the feast phase, since the predicted COD, ammonium, nitrite and nitrate concentrations were similar to the experimental ones (Fig. 3C). During the famine phase, the COD and nitrate profiles were also adequately predicted by the model. In contrast, the model did not completely describe the ammonium and nitrite profiles of the famine phase. The model overestimated the nitrite concentrations and underestimated the ammonium concentration (see Fig. 3C). However, the general trends of both compounds were correctly predicted with the simulation results.

Considering the complexity of the system and the uncertainty of some of the experimental data used as model inputs (e.g. granule size distribution, granules density) it could be considered that the model satisfactorily described the performance of a GSBR treating swine wastewater. Moreover, it is noteworthy that only three kinetic parameters were calibrated while the rest were obtained from literature and, of course,

none of these parameters was changed in the validation. Therefore, the model was ready to start performing other simulations to gain deeper insight into the treatment process.

4.3 Assessment of Nitrogen removal

4.3.1 Effect of the DO and the granule size

The coupled effect of DO and granule size over N-removal was studied using Period A scenario (see details in table 2). The model results for Period A are presented in Fig. 4. For each granule size tested, there was a DO concentration at which N-removal was maximized (DO_{opt}). At DO concentrations higher than the DO_{opt}, ammonium was completely oxidized at the end of the cycle and the N-removal efficiency decreased as DO concentration was increased. N-removal efficiencies at the same DO concentration were higher as higher was the granule size. At DO concentrations below the DO_{opt}, the N-removal efficiency decreased rapidly for lower values of the DO concentration, and ammonium was not completely oxidized at the end of the cycle and accumulated in the effluent.

The DO_{opt} was 2 and 1 mg O_2 L^{-1} for the granule size of 3.5 and 2.0 mm, respectively, and 0.5 mg O_2 L^{-1} for the 1.0 or 0.5 mm, indicating that the DO_{opt} value increased with granule size. Note that for two of the granule sizes (1.0 and 0.5 mm), the DO_{opt} was obtained at the lowest DO concentration used (0.5 mg O_2 L^{-1}), so the decrease of the N-removal at DO concentration lower than the DO_{opt} could not be observed, although it probably occurred at lower DO concentrations.

At the conditions of period A, granules with a granule size between 1 and 2 mm presented better N-removal efficiencies (76 – 80%) than granules with larger (74%) or smaller sizes (71%) at their DO_{opt} (Fig. 4). Noticeably, the variations in N-removal at the DO_{opt} of the different granule sizes were lower than 9%, despite the large range of

granule sizes tested (0.5 – 3.5 mm). Hence, in Period A conditions, applying the adequate DO_{opt} concentration resulted in high N-removal efficiencies independently of the granule size.

4.3.2 Effect of the influent C/N ratio

Two different scenarios, C/N_Low and C/N_High (see table 2), were used to study the effect of the influent C/N ratio over the N-removal. In general, the N-removal efficiencies in both scenarios showed similar trends than those found in period A (Fig. 5). Similarly to Period A, a different DO_{opt} value was determined for each granule size. The values of DO_{opt} for each granule size in C/N_High and C/N_Low scenarios were very similar to those determined in Period A (Fig. 6A). The limitation of the nitrification occurred at a DO concentration close to the DO_{opt}, since, at DO concentration above the DO_{opt}, ammonium was not completely oxidized at the end of the cycle (Fig. 5). Therefore, the influent C/N ratio scarcely influenced the conditions at which N-removal was enhanced. However, the N-removal efficiencies obtained at the same granule size and DO concentrations were, in C/N_High scenario, higher than those in Period A (Fig. 5). In contrast, the N-removal efficiencies in C/N_Low scenario were lower than the corresponding ones in Period A. Therefore, the higher the influent C/N ratio, the higher the N-removal efficiency.

For C/N_High scenario, the higher influent C/N ratio also allowed for good N-removal efficiencies at DO concentrations higher than the DO_{opt}. In fact, granules with a granule size higher than 2 mm and DO concentrations higher than 4 mg O_2 L^{-1} presented N-removal efficiencies higher than 60% (Fig. 5). Maximum N-removal efficiencies of the different granule sizes ranged between 79 and 85% and, similarly to Period A, granules with sizes between 1 and 2 mm presented the best N-removal efficiency (Fig. 6A). In that case, the differences in maximum N-removal at different granule sizes were even

lower than those found for period A, being only 6%. Therefore, with a high influent C/N ratio, there is no need to pay attention to the granule size if the adequate DO_{opt} was applied.

In the C/N_Low scenario, good N-removal efficiencies (71 – 74%) were obtained only for granule sizes between 1 and 2 mm at its corresponding DO_{opt} (0.5 - 1 mg O_2 L^{-1}, Figs. 5 and 6A). For granule sizes 0.5 and 3.5 mm, the N-removal was lower than 60% even at the DO_{opt}. At DO concentrations higher than 4 mg O_2 L^{-1}, N-removal was lower than 36% for all the granule sizes tested (Fig. 5). Note that, even though the low influent C/N ratio negatively affected the N-removal efficiency, good N-removal efficiencies could be obtained applying the adequate DO_{opt} if granule size was between 1 and 2 mm. The maximum N-removal efficiency was only 6 % lower than that in Period A.

4.3.3 Effect of the NLR

The effect of the NLR on the N-removal was also evaluated with the model. One of the advantages of granular reactors is their ability to treat high loading rates due to their high biomass retention capacity [6, 10, 12]. For this reason, the effect of the NLR on the N-removal capacity was studied in two scenarios of 1.5 and 2-fold higher NLR than that applied in period A, maintaining a constant influent C/N ratio (see Table 2).

Simulations results of scenarios NLR_1.5 and NLR_2.0 are presented in Fig. 7. In general, the N-removal performance after increasing the NLR presented similar trends than those found in Period A (see Fig. 7). A DO_{opt} was found for each granule size, where the N-removal was enhanced, and nitrification was limited at a DO concentration close to the DO_{opt} value (Fig. 7). However, the higher the NLR applied, the higher the DO concentration at which the maximum N-removal for each granule size was achieved (i.e., for granule size of 2 mm, the DO_{opt} values were 1, 2 and 3 mg O_2 L^{-1} for scenarios

Period A, NLR1.5 and NLR_2.0, respectively, Fig. 6B). Therefore, for a given granule size, the value of DO_{opt} increased with NLR. This was reasonable, since a reduction of the cycle length resulted in a reduction of the time available for nitrification. Accordingly, higher DO concentrations were needed to increase the thickness of the aerobic layer and, thus, increase the nitrification capacity.

Regarding N-removal efficiencies, the increase of the NLR affected differently the N-removal according to the granule size. At the DO_{opt}, the N-removal efficiency of granules larger than 1 mm decreased with NLR (Fig. 6B). This decrease of N-removal was (4 – 6 %), depending on granule size, but the N-removal efficiency at the DO_{opt} maintained higher than 70% in all cases (Fig. 6B). In contrast, for a granule size of 0.5 mm the N-removal at the DO_{opt} increased with NLR, achieving 80% of N-removal efficiency in the NLR_2.0 scenario. Therefore, in case of an increase of NLR, the lower the granule size, the better the achieved N-removal. Nevertheless, if the DO concentration is maintained at a value close to the DO_{opt}, good N-removal efficiencies could be obtained independently of the granule size.

4.4 Practical implications

4.4.1 Operating guidelines to improve N-removal

The simulation results showed that all the factors taken into account in this study (i.e. DO concentration, particle size, influent C/N ratio and NLR) affected the N-removal. Interestingly, in most of the scenarios tested, the N-removal efficiency could be highly enhanced independently of the rest of the factors, only by applying the adequate DO concentration (i.e. DO_{opt}), thus obtaining N-removal efficiencies higher than 70% (Fig. 6). The only exception was in case of low influent C/N ratio. In that scenario, in

addition to apply the DO_{opt}, a granule size between 1 and 2 mm was needed to obtain good N-removal efficiencies (Fig. 6).

The simulation results also showed that, in all scenarios, the ammonium was completely oxidized at DO concentrations above the DO_{opt}. In contrast, at DO concentrations below the DO_{opt}, ammonium always accumulated in the effluent. This suggested that the limitation of nitrification occurred at a DO concentration close to the DO_{opt} (Figs. 5 and 7). Accordingly, a slight accumulation of ammonium at the end of the cycle (i.e. a slight limitation of the nitrification) would indicate that the DO concentration was close to DO_{opt} and thus, that N-removal was enhanced (Fig. 8). Therefore, it is possible to enhance N-removal simply controlling DO concentration and effluent ammonium concentration. This is very interesting from an operational point of view, since both, DO and ammonium concentrations, are two variables commonly measured on full scale wastewater treatment plants [19] and could easily be controlled. In contrast, granule size is practically uncontrollable in current systems [15], and influent C/N ratio and NLR are related to the wastewater, and therefore subject to variability.

4.4.2 A novel control strategy for enhancing N-removal

A control strategy was proposed based on determining the DO concentration ensuring a slight accumulation of ammonium at the end of each GSBR cycle, which have been found the key to achieve high N-removal efficiencies. The proposed control strategy had a cascade control structure, with a primary control loop of ammonium concentration at the end of the cycle, and a secondary control loop of DO concentration along the aerobic phase of the GSBR (Fig. 9). The manipulated variable of the primary control loop was, consequently, the DO set-point of the secondary loop [38]. The particularity of this control strategy was that the primary ammonium control loop would only act once per cycle. Therefore, after measuring the ammonium concentration at the end of

the cycle, the control loop would establish the DO set-point for the next cycle. The ammonium set-point for the primary loop was set to 5 mg $N\text{-}NH_4^+$ L^{-1}. This set-point was justified by the precision of the current on-line ammonium measurement devices, but also by the importance of having enough range to measure the error between the on-line and set-point ammonium concentrations, in order to calculate the control action (Fig. 8). DO concentration in the reactor should be sufficiently close to the value of DO_{opt} as to obtain high N-removal efficiencies when using 5 mg $N\text{-}NH_4^+$ L^{-1} as ammonium set-point.

The short term effectiveness of the proposed control strategy over the N-removal efficiency was simulated with the model using the conditions applied in Period A with a granule size of 2 mm. To simulate the primary ammonium control loop (Fig. 9), a proportional (P) controller was used [38]. The gain of the P controller was set to 0.25 mg O_2 mg^{-1} $N\text{-}NH_4^+$. The secondary control loop (Fig. 9) was assumed to have a fast response because the control of DO in the model was described with a high gas-liquid oxygen transfer rate (see the details in SI and Jemaat et al. [34]). Before applying the control strategy, the model was run until steady state with a DO concentration of 4 mg O_2 L^{-1}, obtaining complete nitrification at the end of the cycle and 48% of N-removal efficiency (see Fig. 10). Then the control strategy was activated. During the first 36 h after the control activation (12 cycles) the primary ammonium control loop progressively reduced the DO set-point of the secondary DO control loop, until 1 mg O_2 L^{-1}. At that DO concentration, ammonium concentration started to accumulate for the first time in the effluent (Fig. 10). During the next 36 h, the ammonium in the effluent oscillated in the range 1 – 9 mg $N\text{-}NH_4^+$ L^{-1}, producing DO set-point variations between 0.75 and 1.1 mg O_2 L^{-1} (Fig. 10). Seventy-two hours after the start-up of the control strategy, the ammonium concentration in the effluent was finally stabilized at 5 mg N-

NH_4^+ L^{-1}, with a DO concentration of 1.0 mg O_2 L^{-1}. N-removal efficiency after the activation of the control strategy increased from 48% to 75% during the first 36 h (Fig. 10), showing the effectiveness of the control strategy. Moreover, the N-removal efficiency remained stable at 75 ±2 % during the next 36 h (Fig. 10), despite the oscillations of the ammonium in the effluent, showing the robustness of the control strategy.

The most successful approaches to improve N-removal in GSBR previously reported [15,18] were based on changing the cycle structure of the reactor (i. e. adding anoxic periods, dividing the feeding, etc). Here, the proposed control strategy was much simpler, because its implementation maintains the cycle structure, and only the DO set-point was directly manipulated. Furthermore, since the ammonium set-point was established independently of the influent or granular sludge characteristics (e.g. size), automation of the control system is possible and robust, providing stability to the long term operation of the GSBR.

4.4.3 Microbiological risks

The experimental results showed that the enhancement of the N-removal implied, in most cases, to impose low DO concentrations (lower than 2 mg O_2 L^{-1}). Working at such low DO concentrations is advantageous, since the aeration costs could be reduced considerably. However, low DO concentrations may lead to some risks associated to the granules stability. Many authors have pointed out that working at such low DO concentrations may induce an overgrowth of filamentous microorganisms over the granules, which in most cases ended up in granules breakage [12, 14]. Also the use of low aeration rates induced granules instability and final breakdown [17]. Thus, it may be necessary to further study the stability of the granular sludge at the optimal conditions for N-removal.

5. Conclusions

A mathematical model able to describe the operation of a GSBR was successfully calibrated and validated. The subsequent model exploitation revealed that N-removal was always enhanced when the DO applied produced a slight ammonium accumulation in the effluent (e.g. 5 mg $N\text{-}NH_4^+$ L^{-1}). Furthermore, this occurred independently of granule size, influent C/N ratio or NLR. Accordingly, we proposed a cascade ammonium and oxygen control strategy that successfully automates finding the adequate DO concentration to enhance N-removal. The control strategy will set the appropriate DO set-point at whatever values of granule size, influent C/N ratio or NLR. Therefore, high N-removal efficiencies (between 70 – 85%, in most cases) will be assured by the control strategy against disturbances in those variables, which are common during the reactor operation. This is one of the first control strategies proposed for aerobic granular reactors and future research in pilot plant to confirm these results would be desirable.

Acknowledgements

This work has been supported by the Spanish Ministerio de Economía y Competitividad through GRANMADEL/ TOGRANSYS Project (CTQ2008-06792-C02-02/PPQ) and ONLYBIO project (CTQ2011-24745/PPQ).

References

[1] J.J. Beun, A. Hendriks, M.C.M. van Loosdrecht, M. Morgenroth, P.A. Wilderer, J.J. Heijnen, Aerobic granulation in a sequencing batch reactor, Water Res. 33 (1999) 2283 – 2290.

[2] M.K. De Kreuk, M.C.M. van Loosdrecht, Formation of aerobic granules with domestic sewage, J. Environ. Eng. 132 (2006) 694–697.

[3] B. Arrojo, A. Mosquera-Corral, J.M. Garrido, R. Méndez, Aerobic granulation with industrial wastewater in sequencing batch reactors, Water Res. 38 (2004) 3389 – 3399.

[4] S.G. Wang, X.W. Liu, W.X. Gong, B.Y. Gao, D.H. Zhang, H.Q. Yu, Aerobic granulation with brewery wastewater in a sequencing batch reactor, Bioresource Technol. 98 (2007) 2142-2147.

[5] G. Yilmaz, R. Lemaire, J. Keller, Z. Yuan, Simultaneous nitrification, denitrification and phosphorus removal from nutrient-rich industrial wastewater using granular sludge, Biotechnol. Bioeng. 100 (2008) 529–541.

[6] M. Figueroa, Á. Val, J. L. Campos, A. Mosquera-Corral, R. Méndez, Treatment of high loaded swine slurry in an aerobic granular reactor, Water Sci. Technol. 63 (2011) 1808-1814.

[7] M. Coma, M. Verawaty, M. Pijuan, Z. Yuan, P.L. Bond, Enhancing aerobic granulation for biological nutrient removal from domestic wastewater, Bioresource Technol. 103 (2012) 101-108.

[8] Y.Q. Liu, J.H. Tay, State of the art of biogranulation technology for wastewater treatment, Biotechnol. Adv. 22 (2004) 533–563.

[9] S.S. Adav, D.J. Lee, K.Y. Show, J.H. Tay, Aerobic granular sludge: recent advances, Biotechnol. Adv. 26 (2008) 411–423.

[10] M.K. De Kreuk, J.J. Heijnen, M.C.M. van Loosdrecht, Simultaneous COD, nitrogen, and phosphate removal by aerobic granular sludge, Biotechnol. Bioeng. 2 (2005) 761–769.

[11] M.K. Jungles, M. Figueroa, N. Morales, Á. Val, R.H.R. da Costa, J.L. Campos, A. Mosquera-Corral, R. Méndez, Start-up of a pilot scale aerobic granular reactor for organic matter and nitrogen removal, J. Chem. Technol. Biotechnol. 86 (2011) 621-768.

[12] E. Isanta, M.E. Suárez-Ojeda, Á. Val, N. Morales, J. Pérez, J. Carrera, Long term operation of a granular sequencing batch reactor at pilot scale treating a low-strength wastewater, Chem. Eng. J. 198–199 (2012) 136 – 170.

[13] J.J. Beun, M.C.M. Van Loosdrecht, J.J. Heijnen, N-removal in a granular sludge sequencing batch airlift reactor, Biotechnol. Bioeng. 75 (2001) 82–92.

[14] A. Mosquera-Corral, M.K. de Kreuk, J.J. Heijnen, M.C.M. van Loosdrecht, Effects of oxygen concentration on N-removal in an aerobic granular sludge reactor, Water Res. 39 (2005) 2676 – 2686.

[15] M.K. De Kreuk, C. Picioreanu, M. Hosseini, J.B. Xavier, M.C.M. van Loosdrecht, Kinetic model of a granular sludge SBR: Influences on nutrient removal, Biotechnol. Bioeng. 97 (2007) 801–815.

[16] J.H. Tay, S. Pan, Y.X. He, Effect of Organic Loading Rate on Aerobic Granulation II: Characteristics of Aerobic Granules, J. Environ. Eng. 130 (2004) 1102 – 1109.

[17] J.H. Tay, Q.S. Liu, Y. Liu, The effect of upflow air velocity on the structure of aerobic granules cultivated in a sequencing batch reactor, Water Sci. Technol. 49 (11 – 12) (2004) 35 – 40.

[18] F.Y. Chen, Y.Q. Liu, J.H. Tay, P. Ning, Operational strategies for nitrogen removal in granular sequencing batch reactor, J. Hazard. Mater. 189 (2011) 342 – 348.

[19] G. Olsson, ICA and me – A subjective review, Water Res. 46 (2012) 1585 – 1624.

[20] N. Kishida, J. Kim, S. Tsuneda, R. Sudo, Anaerobic/oxic/anoxic granular sludge process as an effective nutrient removal process utilizing denitrifying polyphosphate-accumulating organisms, Water Res. 40 (2006) 2303–2310.

[21] S.S. Adav, D.J. Lee, J.Y. Lai, Biological nitrification–denitrification with alternating oxic and anoxic operations using aerobic granules, Appl. Microbiol. Biotechnol. 84 (2009) 1181–1189.

[22] J.A. Torà, E. Moliné, J. Carrera, J. Pérez, Efficient and automated start-up of a pilot reactor for nitritation of reject water: From batch granulation to high rate continuous operation, Chem. Eng. J. 226 (2013) 319-325.

[23] S. López-Palau, A. Pinto, N. Basset, J. Dosta, J. Mata-Álvarez, ORP slope and feast-famine strategy as the basis of the control of a granular sequencing batch reactor treating winery wastewater, Biochem. Eng. J. (2012) 190 – 198.

[24] X. Yuan, D. Gao, Effect of dissolved oxygen on nitrogen removal and process control in aerobic granular sludge reactor, J. Hazard Mater. 178 (2010) 1041-1045.

[25] K.Z. Su, H.Q. Yu, A generalized model for aerobic granule-based sequencing batch reactor. 1. Model development, Environ. Sci. Technol. 40 (2006) 4703–4708.

[26] B.J. Ni, H.Q. Yu, Y.J. Sun, Modeling simultaneous autotrophic and heterotrophic growth in aerobic granules, Water Res. 42 (2008) 1583–1594.

[27] J.R. Vázquez-Padín, A. Mosquera-Corral, J.L. Campos, R. Méndez, J. Carrera, J. Pérez, Modelling aerobic granular SBR at variable COD/N ratios including accurate description of total solids concentration, Biochem. Eng. J. 49 (2010) 173-184.

[28] K.Z. Su, B.J. Ni, H.Q. Yu, Modeling and Optimization of granulation process of activated sludge in sequencing batch reactors, Biotechnol Bioeng. 110 (2013) 1312 - 1322.

[29] P. Reichert, AQUASIM 2.0 - Computer program for the identification and simulation of aquatic systems, Swiss Federal Institute of Environmental Science and Technology (EAWG), Switzerland, 1998.

[30] M. Henze, W. Gujer, T. Mino, M.C.M. van Loosdrecht, Activated Sludge Models ASM1, ASM2, ASM2d, and ASM3, IWA Scientific and Technical Report No. 9, IWA Publishing, London, UK, 2000.

[31] G. Sin, A. Guisasola, D.J.W. de Pauw, J.A Baeza, J. Carrera, P.A. Vanrolleghem, A new approach for modelling simultaneous storage and growth processes for activated sludge systems under aerobic conditions, Biotechnol. Bioeng. 92 (2005) 600-613.

[32] I. Jubany, J. Carrera, J. Lafuente, J.A. Baeza, Start-up of a nitrification system with automatic control to treat highly concentrated ammonium wastewater: Experimental results and modeling, Chem. Engin. J. 144 (2008) 407–419.

[33] D. Kaelin, R. Manser, L. Rieger, J. Eugster, K. Rottermann, H. Siegrist, Extension of ASM3 for two-step nitrification and denitrification and its calibration and validation with batch tests and pilot scale data, Water Res. 43 (2009) 1680-1692.

[34] Z. Jemaat, A. Bartrolí, E. Isanta, J. Carrera, M.E. Suárez-Ojeda, J. Pérez, Closed-loop control of ammonium concentration in nitritation: Convenient for reactor operation but also for modeling, Bioresource Technol. 128 (2013) 655–663.

[35] J.J. Beun, M.C.M. van Loosdrecht, J.J. Heijnen, Aerobic granulation in a sequencing batch airlift reactor, Water Res. 36 (2002) 702–712.

[36] G. Sin, D. Kaelin, M.J. Kampschreur, I. Takacs, B. Wett, K.V. Gernaey, L. Rieger, H. Siegrist, M.C.M. van Loosdrecht, Modelling nitrite in wastewater treatment systems: a discussion of different modelling concepts, Water Sci. Technol. 58 (2008) 1155 – 1171.

[37] G. Munz, C. Lubello, J. Oleszkiewicz, Factors affecting the growth rates of ammonium and nitrite oxidizing bacteria, Chemosphere 83 (2011) 720-725.

[38] G. Stephanopoulos, Chemical process control: an introduction to theory and practice, Prentice-Hall, Upper Saddle River, New Jersey, 1984.

FIGURE CAPTIONS

Figure 1. Time course concentrations of ammonium, nitrite and nitrate as experimentally measured in the lab-scale GSBR. Experimental data obtained in period A were used for the calibration of the model. Results of the model at the operating conditions established in period C were used to validate the model.

Figure 2. Example of the effect of using a reduction factor on the diffusion coefficient of soluble compounds on model COD predictions during the first 60 minutes of a cycle. The reduction factor (μ_D) is only active during the first 3 minutes of each cycle (minute 0 to 3 in the graph), which corresponds to the static (non-aerated) feeding phase of the GSBR.

Figure 3. Time course concentrations of N-species (A,C) and COD (B,D) in a cycle as measured experimentally (symbols) compared to those predicted by the model (lines). A and B figures correspond to the calibration and C and D figures correspond to the validation.

Figure 4. Simulated N-removal efficiencies and effluent ammonium concentrations predicted by the model at different DO concentrations in the bulk liquid and at different granule sizes (dp). Simulations were performed under the operating conditions defined for Period A scenario, as detailed in table 2.

Figure 5. Simulated N-removal efficiencies and effluent ammonium concentrations predicted by the model at different DO concentrations in the bulk liquid and at different granule sizes (dp). Simulations were performed under the GSBR conditions defined for C/N_Low (left) and C/N_High (right) scenarios, as detailed in table 2.

Figure 6. Comparison of the maximum N-removal efficiencies and DO_{opt} obtained at the different granule sizes for C/N_Low, C/N_High and Period A scenarios (A); and NLR_1.5, NLR_2.0 and Period A scenarios (B).

Figure 7. Simulated N-removal efficiencies and effluent ammonium concentrations predicted by the model at different DO concentrations in the bulk liquid and at different granule sizes (dp). Simulations were performed under the GSBR conditions for NLR_1.5 (left) and NLR_2.0 (right) scenarios, as detailed in table 2.

Figure 8. Schematic representation of the effluent concentration of N-species and N-removal obtained at different DO concentrations. The DO_{opt} value and the DO range with high N-removal efficiency are highlighted with a dotted line and grey band, respectively.

Figure 9. Block-diagram of the cascade control strategy proposed to enhance the N-removal. The primary loop only acts once per cycle, using the ammonium concentration at the end of one cycle (effluent concentration) to establish the DO set-point value of the next cycle. The secondary loop is only active during the aerobic phase of the GSBR cycle, and DO set-point is maintained constant during the whole aerobic phase.

Figure 10. DO concentration during aerobic phase, effluent ammonium concentration (end of the cycle) and N-removal efficiencies before and after applying the proposed cascade control strategy in the GSBR. The ammonium set-point was 5 mg $N\text{-}NH_4^+$ L^{-1}. Since the secondary DO control loop was supposed to be fast and efficient, the represented DO concentration after the control strategy activation is equal to the DO set-point value

TABLES

Table 1. Experimental data related to the influent composition and biomass characteristics in Periods A and C, used as model inputs to simulate the GSBR operation for the calibration and validation.

	Period A (Calibration)	Period C (Validation)
Influent characteristics		
Readily-biodegradable COD (mg O_2 L^{-1})	600	1000
Non–biodegradable COD (mg O_2 L^{-1})	60	116
Ammonium (mg N L^{-1})	103	200
Influent C/N ratio (g O_2 g^{-1} N)	5.8	5
Granules characteristics		
Volume-weighted average granule size (mm)	3.55	3.13
Biomass concentration (g VSS L^{-1})	5	11.5
Density (g VSS $L^{-1}_{granule}$)	25	37
Number of granules	12806	29301

Table 2. Characteristics of the scenarios used for the model exploitation

	$COD_{influent}$	$NH_4^+{}_{influent}$	C/N	VSS	HRT	NLR_V	NLR_S
	(mg O_2 L^{-1})	(mg N L^{-1})	(g O_2 g^{-1} N)	(g L^{-1})	(h)	(g N L^{-1} d^{-1})	(g N g^{-1} VSS d^{-1})
Period A	600	103	5.8	5	6	0.41	0.082
C/N_High	1030	103	10	5	6	0.41	0.082
C/N_Low	412	103	4	5	6	0.41	0.082
NLR_1.5	600	103	5.8	5	4	0.61	0.123
NLR_2.0	600	103	5.8	5	2	0.82	0.164

FIGURES

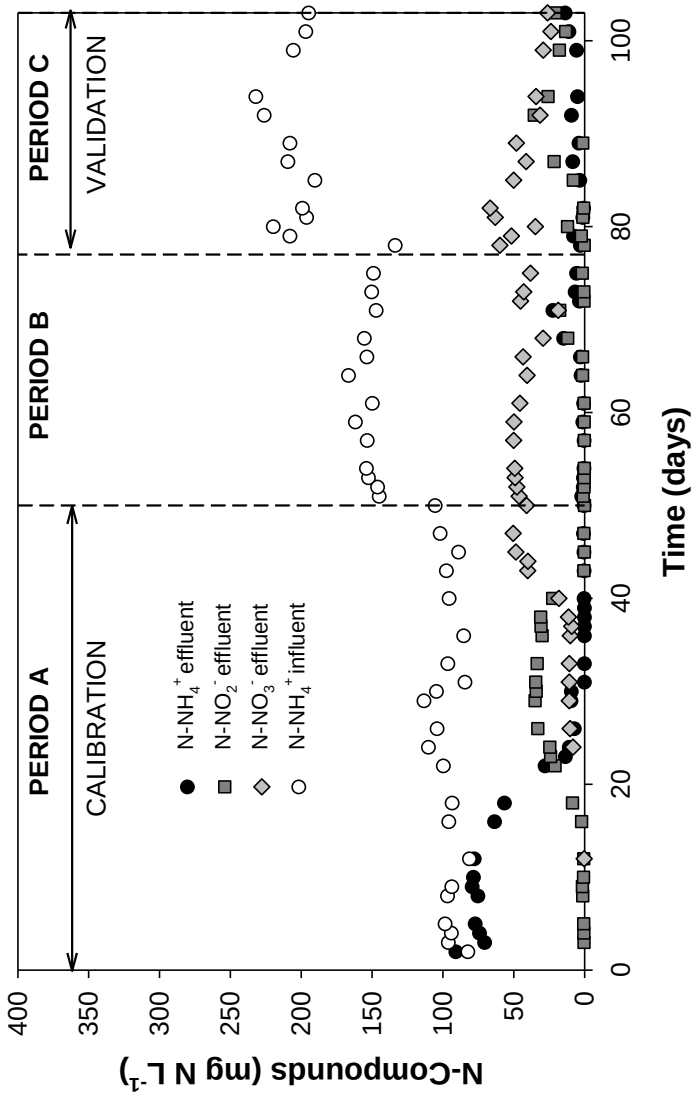

Figure 1.

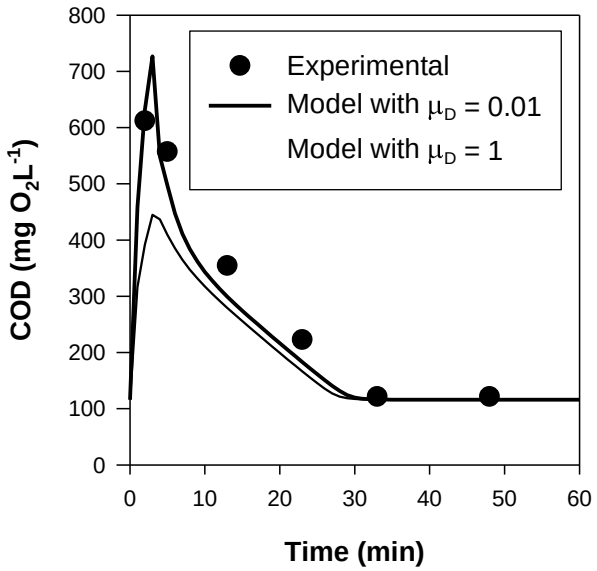
800
700
600
500
400
300
200
100
0
0
10
20
30
40
50
60
COD (mg O2L-1)
Time (min)
Experimental
Model with μD = 0.01
Model with μD = 1

Figure 2.

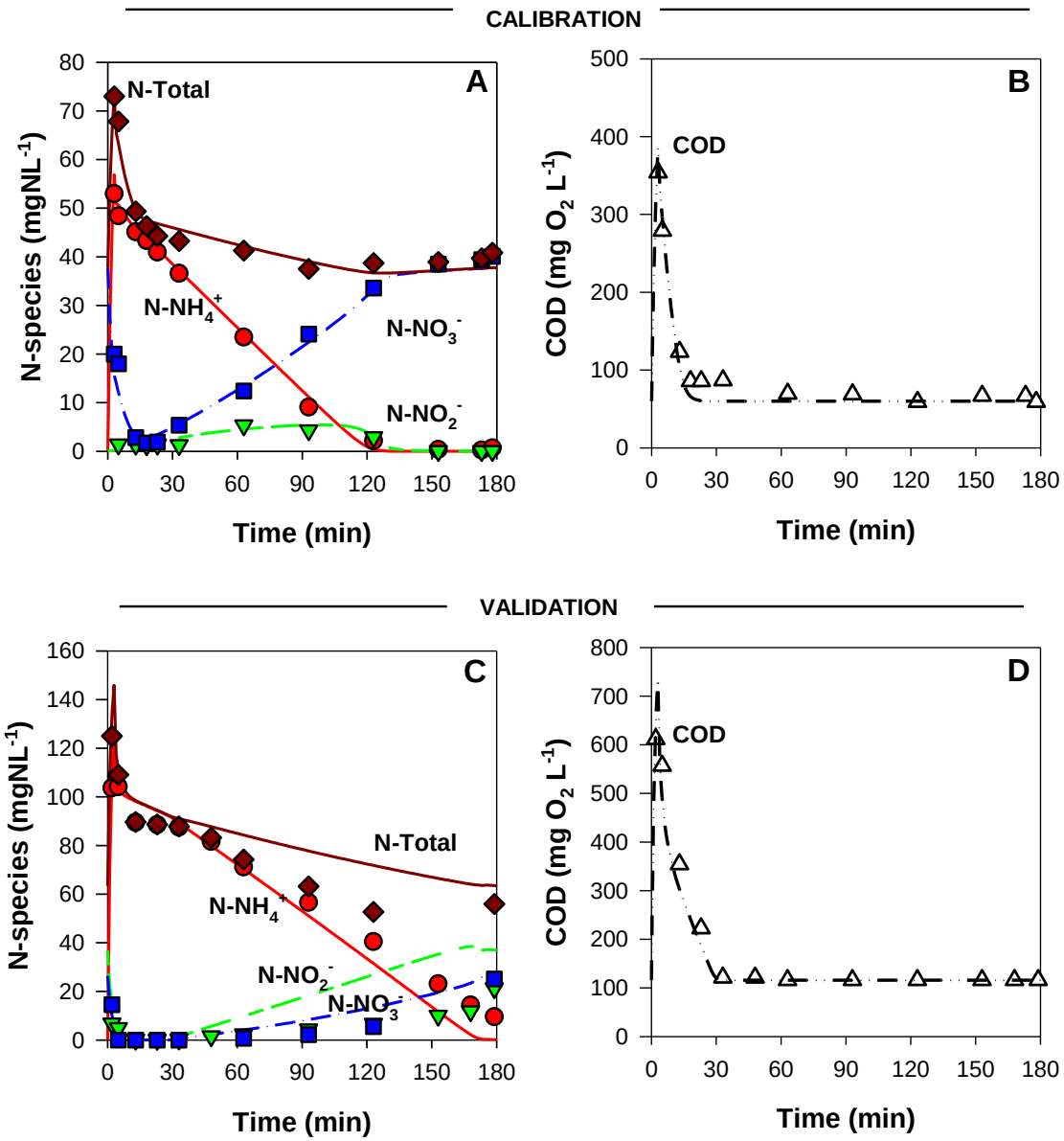
CALIBRATION
A
N-Total
N-NH4+
N-NO3-
N-NO2-
N-species (mgNL-1)
Time (min)
B
COD
COD (mg O2 L-1)
Time (min)
VALIDATION
C
N-Total
N-NH4+
N-NO2-
N-NO3-
N-species (mgNL-1)
Time (min)
D
COD
COD (mg O2 L-1)
Time (min)

Figure 3.

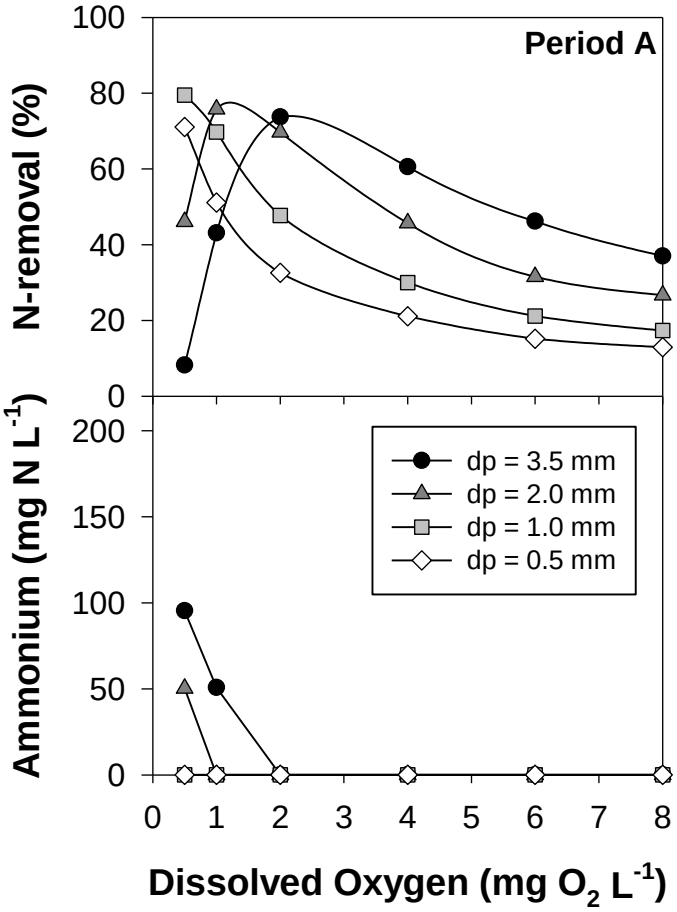
Period A
N-removal (%)
Ammonium (mg N L-1)
dp = 3.5 mm
dp = 2.0 mm
dp = 1.0 mm
dp = 0.5 mm
Dissolved Oxygen (mg O2 L-1)

Figure 4.

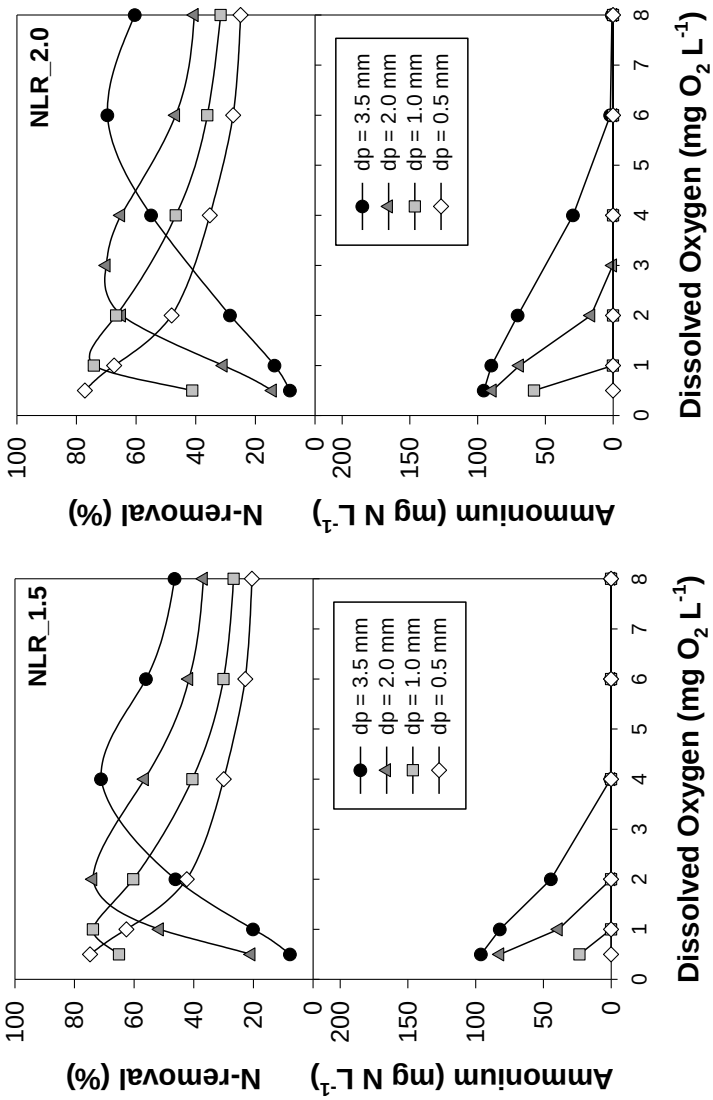
NLR_2.0
NLR_1.5
N-removal (%)
Ammonium (mg N L-1)
Dissolved Oxygen (mg O2 L-1)
dp = 3.5 mm
dp = 2.0 mm
dp = 1.0 mm
dp = 0.5 mm

Figure 5

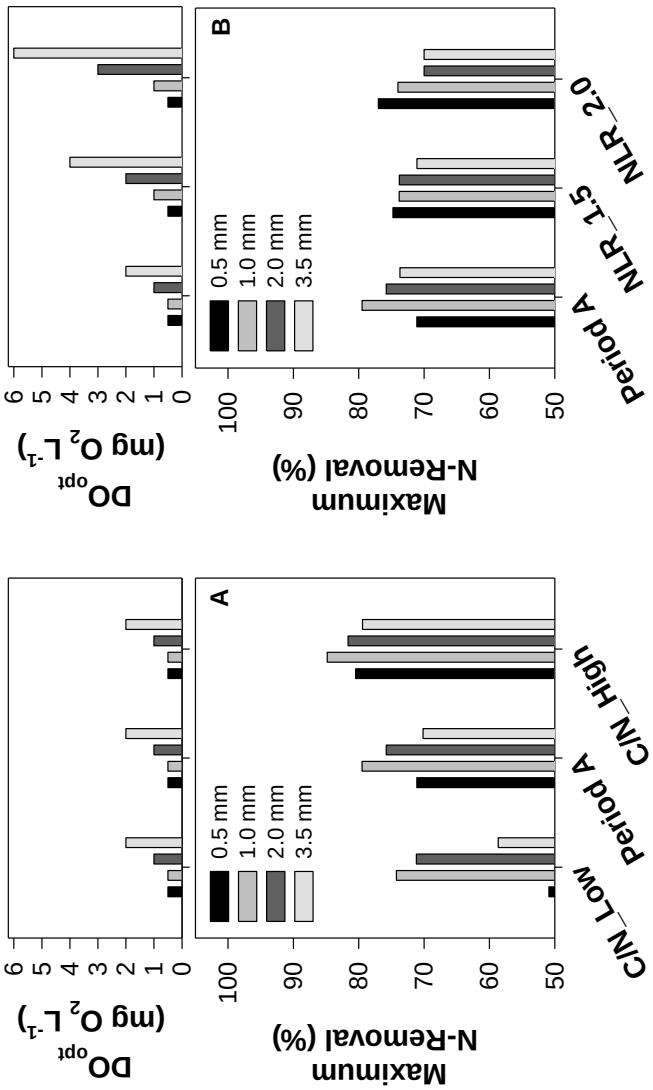
A
B
0.5 mm
1.0 mm
2.0 mm
3.5 mm
Maximum
N-Removal (%)
DO$_{opt}$
(mg O$_2$ L^{-1})
C/N_Low
Period A
C/N_High
NLR_1.5
NLR_2.0

Figure 6.

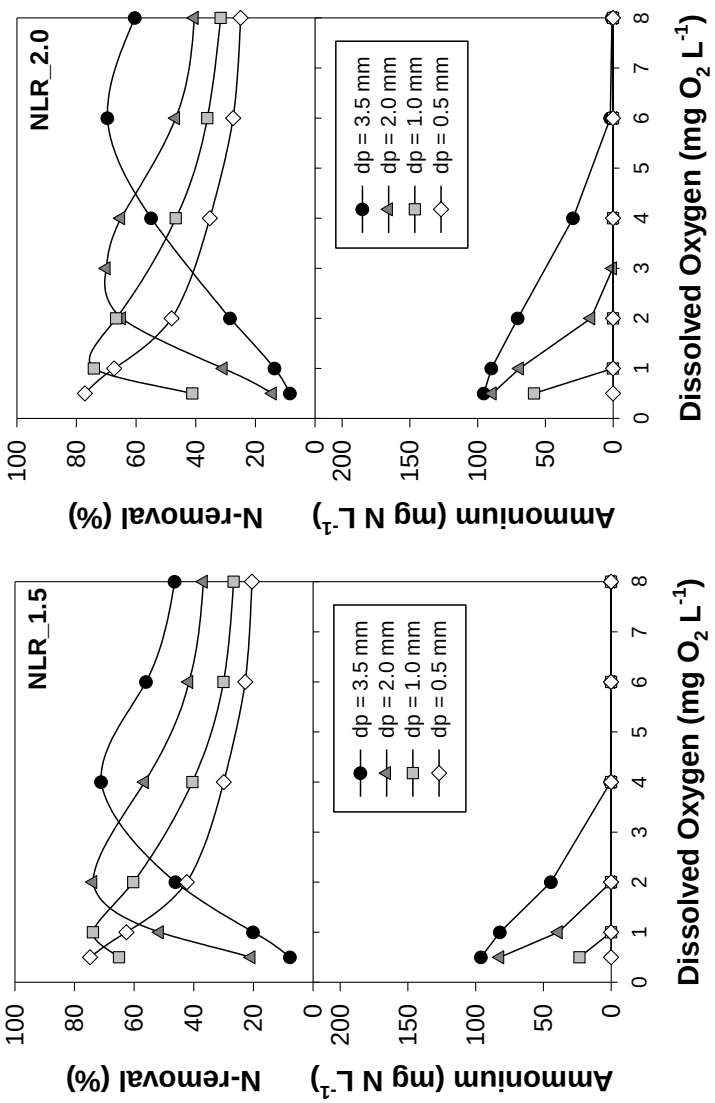
NLR_2.0
NLR_1.5
N-removal (%)
Ammonium (mg N L-1)
Dissolved Oxygen (mg O2 L-1)
dp = 3.5 mm
dp = 2.0 mm
dp = 1.0 mm
dp = 0.5 mm

Figure 7

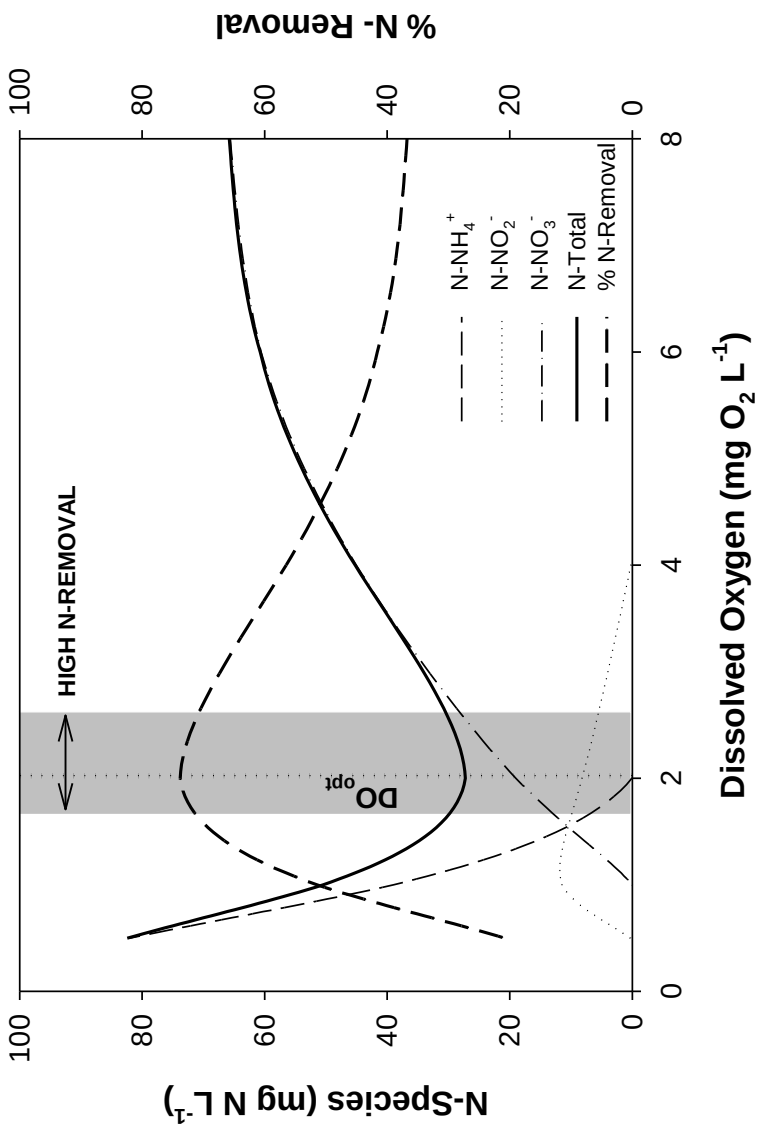
N-Species (mg N L-1)
% N- Removal
Dissolved Oxygen (mg O2 L-1)
HIGH N-REMOVAL
DOopt
N-NH4+
N-NO2-
N-NO3-
N-Total
% N-Removal
0
20
40
60
80
100
0
2
4
6
8

Figure 8.

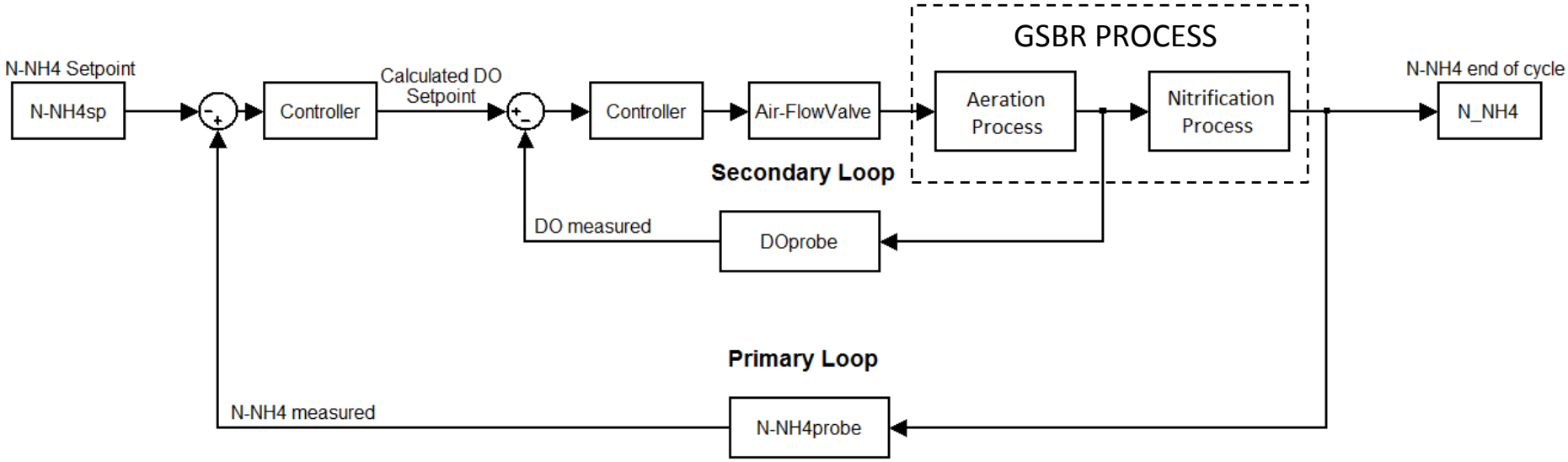
GSBR PROCESS
N-NH4 Setpoint
N-NH4sp
Controller
Calculated DO Setpoint
Controller
Air-FlowValve
Aeration Process
Nitrification Process
N-NH4 end of cycle
N_NH4
Secondary Loop
DO measured
DOprobe
Primary Loop
N-NH4 measured
N-NH4probe

Figure 9

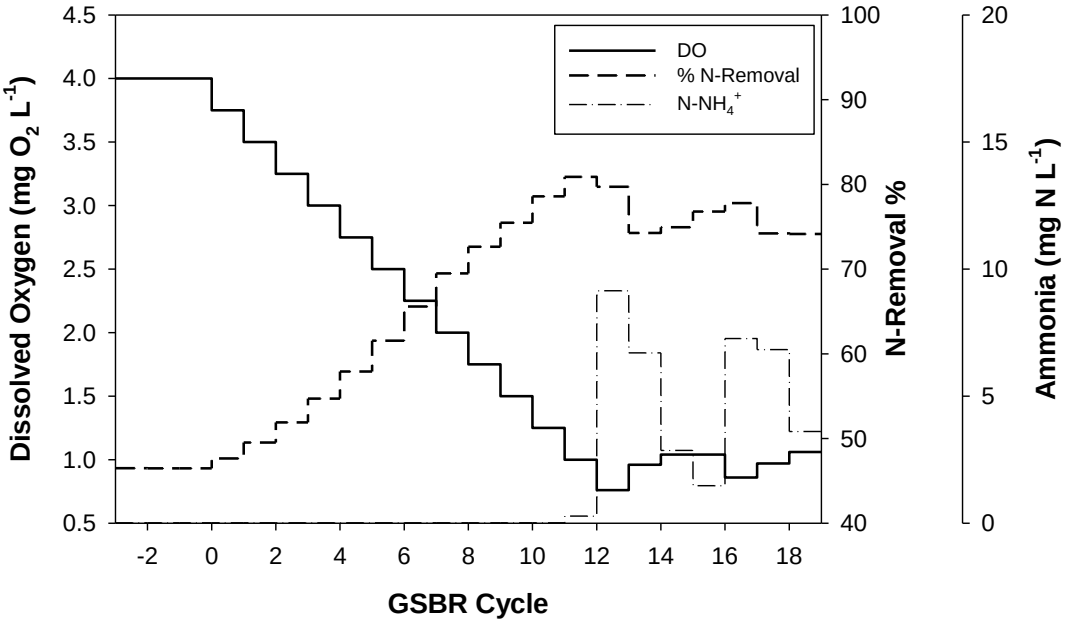
DO
% N-Removal
N-NH4+
Dissolved Oxygen (mg O2 L-1)
N-Removal %
Ammonia (mg N L-1)
GSBR Cycle
4.5
4.0
3.5
3.0
2.5
2.0
1.5
1.0
0.5
100
90
80
70
60
50
40
20
15
10
5
0
-2
0
2
4
6
8
10
12
14
16
18

Figure 10.